IEEE Access
Multidisciplinary | Rapid Review | Open Access Journal

Received March 22, 2021, accepted April 6, 2021, date of publication April 13, 2021, date of current version April 21, 2021.

Digital Object Identifier 10.1109/ACCESS.2021.3072935

The Identification and Compensation of Static Drift Induced by External Disturbances for LiDAR SLAM

DA LI, BIN ZHOU, ZHANGYU WANG, SONGYUE YANG, AND PENGFEI LIU

School of Transportation Science and Engineering, Beihang University, Beijing 100191, China
Key Laboratory of Autonomous Transportation Technology for Special Vehicles, School of Transportation Science and Engineering, Ministry of Industry and Information Technology, Beihang University, Beijing 100191, China

Corresponding author: Zhangyu Wang (zywang@buaa.edu.cn)

This work was supported in part by the National Natural Science Foundation of China under Grant 52072020, and in part by the Beijing Natural Science Foundation under Grant L191002.

ABSTRACT With the extending use of LiDAR SLAM in various areas, the interference of external disturbances on SLAM is becoming more and more obvious. Huge efforts have been made to reduce the drift error of LiDAR SLAM using graph-based methods. However, the mapping results can be severely affected by external disturbances under extreme conditions, which will limit the performance of graph-based methods. This study proposes a new strategy to reduce the static drift on a local scale by identifying and compensating the influence of external disturbances based on the localization results of LiDAR SLAM. Contrast experiments were first designed and performed to analyze the potential inducing factors of static drift, such as environment and vibration. The Kalman filter was adopted to estimate the speed and acceleration parameters based on the localization results of LiDAR SLAM. Then, an estimation criterion of static drift was established according to the interference of external disturbances on speed and acceleration. Finally, a static drift compensation method for LiDAR SLAM was proposed to compensate the drift of the pose. In the verification experiment, for 1866 data points, the identification accuracy of static drift was 97.32%, and the final positioning error of LiDAR SLAM was reduced from 4.9464 m to 0.1741 m after the compensation of static drift.

INDEX TERMS LiDAR SLAM, external disturbance, static drift, Kalman filter, parameter estimation, pose compensation.

I. INTRODUCTION

Simultaneous localization and mapping (SLAM) based on light detection and ranging (LiDAR) has been applied to various areas such as autonomous cars, aerial survey [1], agriculture [2], forestry [3], and heritage mapping [4]. Great efforts have been made to reduce the positioning error of SLAM, which is commonly represented as the drift of trajectory.

One of the main tasks of LiDAR SLAM is to achieve an accurate matching based on point cloud. Iterative closest point (ICP) is one of the typical methods to find the transformation between different LiDAR scans [5]. Two sets of points are matched iteratively until stopping criteria are satisfied in ICP. However, if the scans contain a large number of points, the computational cost at the point level will increase rapidly. Therefore, feature-based scan matching methods have been proposed, which mainly focused on the key points, sharp corners, edge lines, and planar surfaces in the point cloud. Zhang and Singh [6] and [7] proposed a low-drift and real-time lidar odometry and mapping (LOAM) method with an outstanding performance. In LOAM, feature points on sharp edges and planar surface patches were extracted from the point cloud. Edge points of the source cloud were matched with the edge lines in the target cloud, while planar points were matched with planar surface patches.

With the extending use of LiDAR SLAM in various areas, the interference of external disturbances on SLAM is becoming more and more obvious. Besides the ranging measurement error and the orientation error, mechanical vibration is also one potential interfering factors of LiDAR under certain conditions. Li *et al.* [8] pointed out that platform vibration error is one of the typical missile-borne LiDAR

The associate editor coordinating the review of this manuscript and approving it for publication was Hassen Ouakad.

errors, that cannot be ignored. In aerial LiDAR measurements, Kolecki *et al.* [9] pointed out that the presence of vibrations from the rotors and engines of a gyrocopter had disturbing impacts on the laser point pattern. In the research conducted by Canata *et al.* [2], LiDAR was used to assess the height of sugarcane plants during the pre-harvest period. The influence of vibration on the performance of LiDAR under field conditions was found to be significant. Luo and Li [10] indicated that the impact of vibration on cross slope measurement was not negligible and needed to be calibrated in the measurement for highway ramps using inertial measurement unit (IMU) and three-dimension (3D) LiDAR. Research by Periu *et al.* [11] has shown that the LiDAR sensor installed on an agricultural tractor is affected by the mechanical vibrations induced by the operation of the tractor on uneven terrain. Vibrations on different unmanned aerial vehicle (UAV) platforms and under different working conditions are compared by Li *et al.* [4] to find an appropriate UAV to carry a LiDAR system for heritage mapping. The piston engine was found to be the primary source of a helicopter's vibration, constituting a major interference for the LiDAR system. Attentions have been drawn upon the influence of vibration on LiDAR.

There are different ways to address the interference of external disturbances on LiDAR SLAM. One way is to employ graph-based optimization methods [12] in the SLAM framework to enhance the performance of SLAM. Among all the back-end optimization strategies, loop closure detection and ground detection are two popular methods that can reduce the drift error. The detection of loop closure is aimed to establish the relationship between current data and previous data as a constraint in the optimization when the current environment is verified as a visited environment. Loop closure detection has been applied to multiple scenarios to eliminate the drift on a global scale [13]–[15]. In lightweight and ground-optimized LOAM (LeGO-LOAM) [16], ground detection was adopted to reduce drift error for ground vehicles. Ground point was separated from point cloud and planar features extracted from the ground were used to obtain $(p_z, p_{\text{roll}}, p_{\text{pitch}})$. Another way is to mitigate a certain external disturbance by mechanical approaches outside the SLAM framework. Pu *et al.* [17] proposed a multi-layer electromagnetic spring with tunable negative stiffness to attenuate the vibration of the LiDAR.

However, when the LiDAR SLAM is applied to extreme conditions, the point cloud map constructed in SLAM could be affected by external disturbances, and mechanical measures might not be able to eliminate all external disturbances for practical reasons. Since external disturbances such as vibration will always leave traces on the localization results of LiDAR SLAM, it is possible to solve the problem from a new angle by identifying and compensating the influence of external disturbances based on the localization results instead of map. These identification and compensation methods independent from point cloud map can provide a new strategy in extending the use of LiDAR SLAM to various fields.

Although LiDAR is a unique sensor with several advantages over the traditional inertial sensors, the basic principles of how LiDAR SLAM works in localization are similar to other sensors. Kalman filter (KF) and its variants are usually employed to estimate the drift error in inertial sensors such as IMU [18]–[20], MEMS IMU [21], [22], and fiber optic gyroscope [23]–[25]. After the identification and estimation of drift error, the compensation method can be implemented accordingly. The same idea is also promising to be applied to the identification and compensation of drift error for the LiDAR SLAM.

The first idea of this work is to analyze the potential inducing factors of the drift error on a local scale by contrast experiments. According to the motion state of the platform, drift error can be classified as static drift and dynamic drift. This study mainly focused on the static drift of LiDAR SLAM when the platform is at a static pose without any translation and rotation. Contrast experiments on potential inducing factors are designed and performed in indoor environments to exclude unrelated external disturbances.

The drift error of SLAM induced by external disturbances can be severe under extreme conditions. Due to the interference of static drift on mapping procedure in SLAM algorithm, graph-based strategies, such as loop closure detection and ground detection, will be limited to eliminate the drift error of the map. Therefore, the second idea of this work is to propose a new strategy to identify the existence of static drift based on the localization results of SLAM and compensate the static drift.

The remainder of this paper is structured as follows: Details of the experimental description are explained in Section 2. The potential inducing factors of static drift are investigated on the basis of contrast experiments in Section 3. The identification of static drift using parameter estimation based on KF is introduced in Section 4. In Section 5, a compensation algorithm for static drift is proposed and verified by experimental data. In Section 6, the influences of static drift on loop closure detection and ground detection are discussed. Finally, conclusions are given in Section 7.

II. EXPERIMENT DESCRIPTION

A. EXPERIMENTAL PLATFORM

An unmanned ground vehicle (UGV) mounted with a LiDAR sensor was used in experiments, as shown in Figure 1. The UGV platform, SCOUT 2.0, is a four-wheel differential steered chassis with a maximum linear speed of 1.5 m/s and a maximum angular speed of 0.5235 rad/s. The LiDAR is Velodyne-16 (VLP-16) with a measurement range up to 100m and an accuracy of ± 3 cm. The vertical angular resolution is 2° and the horizontal angular resolution varies from 0.1° to 0.4°. The vertical field of view of the LiDAR is 30° (±15°). A box PC with an Intel i7-6820EQ CPU was used to run the SLAM framework.

B. SLAM ALGORITHM

As one of the state-of-the-art algorithms for LiDAR SLAM, LOAM [6], [7] achieved a high level of accuracy in the KITTI

FIGURE 1. UGV platform.

dataset. The key idea of LOAM was to match sharp points and planar points of the current scan to edge lines and planar surfaces of the previous scan, respectively. Hence, when the point cloud in the environment is distributed unevenly, the localization accuracy of LOAM could be affected. In this study, the features of static drift for LOAM in typical indoor scenarios were investigated.

The LiDAR coordinate system is a 3D coordinate system with its origin at the geometric center of the LiDAR. The typical convention to specify the reference system in vehicles is used, i.e.: the x-axis is pointing forward, the y-axis is pointing to the left, and the z-axis is pointing upward. The world coordinate system is a 3D coordinate system corresponding with the LiDAR coordinate system at the initial pose.

C. TESTING ENVIRONMENT AND PROCEDURE

All the data were collected in an office and a corridor as illustrated in Figure 2. The experiments were performed without the interference of dynamic objects in the environment.

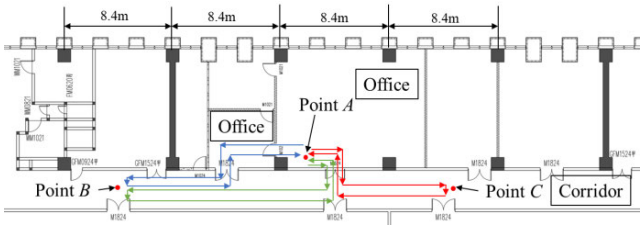

FIGURE 2. Testing environment and the schematic diagram of experiments. (In Experiment 2, the course of the second moving phase is indicated by green arrows. In Experiment 3, the course of the second moving phase is indicated by red arrows and the course of the fourth moving phase is indicated by blue arrows).

The static drift at point A can be observed in the office. The UGV will stay for a period of time and then move out of the office. After moving along the corridor to reach point B or point C, the UGV will finally move back to point A in the office. Therefore, the influence of static drift on LiDAR SLAM can be assessed using the data collected throughout the process.

Four sets of experiments were designed and carried out. In Experiment 1, the UGV was kept stationary at point A and point B for 5 minutes, respectively, to investigate how the environment influences the static drift.

Experiment 2 is a two-phase experiment which was designed to evaluate the influence of static drift on SLAM. In the first static phase, the UGV was kept stationary at point A for 50 seconds, while in the second moving phase, the UGV moved out of the office from point A, then moved along the corridor to reach point B, and finally moved back to point A in the initial pose. The course of the second moving phase in Experiment 2 is indicated by green arrows in Figure 2.

Experiment 3 is a four-phase experiment that was performed to verify the identification and compensation methods of static drift for LiDAR SLAM. In the first static phase, the UGV was kept stationary at point A for 50 seconds. In the second moving phase, the UGV moved along the corridor to reach point C and moved back to point A. In the third static phase, the UGV was kept stationary at point A for an additional 50 seconds. In the fourth moving phase, the UGV reached point B and moved back to point A. As shown in Figure 2, the course of the second moving phase is indicated by red arrows and the course of the fourth moving phase is indicated by blue arrows.

Experiment 4 is the continuous repetition of Experiment 2 procedure two times. The UGV was kept stationary at point A for 50 seconds. Then the UGV moved into the corridor to reach point B and then moved back to point A. After being kept stationary at point A for another 50 seconds, the UGV moved into the corridor for the second time to reach point B and moved back to point A. The point cloud map of corridor was constructed twice in Experiment 4, and the interference in the mapping procedure caused by static drift will be discussed in Section 6.

In Experiment 2, Experiment 3, and Experiment 4, the UGV all started from point A with the initial pose of $(x, y, z, yaw, pitch, roll) = (0, 0, 0, 0, 0, 0)$ for the LiDAR SLAM. In the end of the experiments, the UGV all were all restored to the initial pose at point A. Therefore, the 6-DoF output of LiDAR SLAM at the end of the experiment can be taken as the cumulative positioning error of the whole process.

III. INDUCING FACTORS OF STATIC DRIFT

A. CONTRAST EXPERIMENTS ON ENVIRONMENT

The distribution of point cloud plays an important role in LiDAR SLAM. The features of point cloud distribution are different in the office and the corridor. At point A in the office, feature points are distributed unevenly with only a small proportion of feature points on the ceiling (Figure 3). However, feature points are more uniformly distributed on the surfaces in all directions at point B (Figure 4) and point C (Figure 5) in the corridor.

In Experiment 1, the output data of LiDAR SLAM at point A and point B were obtained with the UGV in a stationary state for 5 minutes. As shown in Figure 7, the positioning

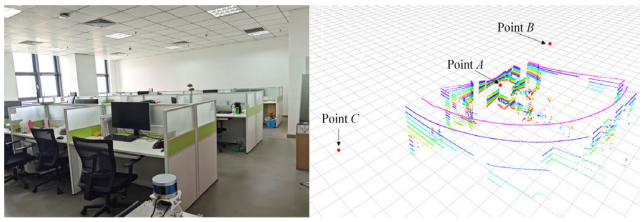

FIGURE 3. Environment and point cloud at point *A*.

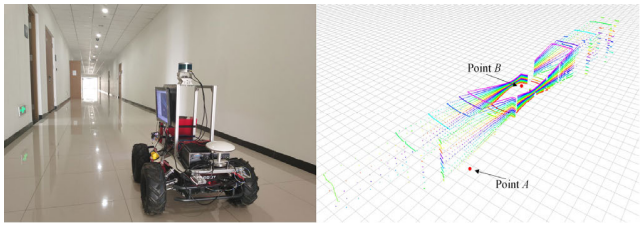

FIGURE 4. Environment and point cloud at point *B*.

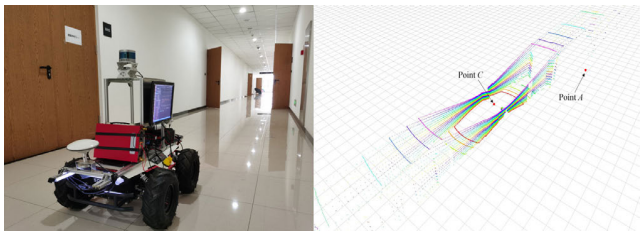

FIGURE 5. Environment and point cloud at point *C*.

results of LiDAR SLAM is drifting at an average speed of 0.0333 m/s at point *A*. Nevertheless, in Figure 8, static drift can hardly be observed at point *B*. The 3D trajectory of LiDAR SLAM at point *A* is shown in Figure 6. Therefore, the distribution of point cloud in the environment has a significant impact on the static drift. In this paper, the identification and compensation methods are focused on the static drift induced in the office around point *A*. From the contrast experiments on environment, it can be concluded that evenly distributed point cloud can restrict the static drift.

B. CONTRAST EXPERIMENTS ON MECHANICAL VIBRATION

A LiDAR mounted on a platform must endure the mechanical vibrations from the engines, rotors, wind, etc. Different kinds of vibration-control equipment have been developed for LiDAR on different platforms [9], [11], [17]. The influence of vibration on the distribution of point cloud has been observed in experiments [17].

When the LiDAR evaluates its position on a static but vibrating platform, the difference between the frequency of LiDAR operation and the frequency of platform vibration will possibly create positioning errors from scan to scan for the LiDAR SLAM. The positioning errors induced by the vibration can accumulate with time, which can be observed as static drift.

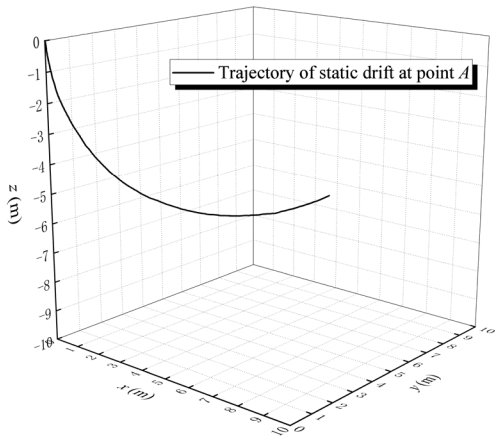

FIGURE 6. The trajectory of LiDAR SLAM at point *A* in Experiment 1.

Besides all the mechanical vibrations from the platform, the vibration from the sensor itself should not be neglected as well. When the VLP-16 LiDAR operates, the motor inside will rotate at a speed of 600 r/min. As shown in Figure 9, a WT61PC IMU is mounted on the top of LiDAR to measure the mechanical vibration during operation. The bias stability of the IMU is 0.01 g in acceleration and 0.05 °/s in angular velocity. The sampling frequency of IMU can be set from 0.1 Hz to 200 Hz.

Evident differences in acceleration data can be observed when the LiDAR was off and on respectively, as shown in Figure 10 and Figure 11. The average values of acceleration on x-axis, y-axis, z-axis were 0.1249 m/s^2, -0.1833 m/s^2, 9.7710 m/s^2 when the LiDAR was off, and the average values of acceleration on x-axis, y-axis, z-axis were 0.1230 m/s^2, -0.1845 m/s^2, 9.7750 m/s^2 when the LiDAR was on. The standard deviations of acceleration on x-axis, y-axis, z-axis were 0.0031 m/s^2, 0.0031 m/s^2, 0.0037 m/s^2 when the LiDAR was off, and the standard deviations of acceleration on x-axis, y-axis, z-axis were 0.0464 m/s^2, 0.0152 m/s^2, 0.0067 m/s^2 when the LiDAR was on. An increase in the standard deviations of accelerations can be an indicator for the existence of the vibration generated by LiDAR itself.

For contrast, the LiDAR was switched onto a static heavy shelf at point *A* with more constrains for the vibration. When the LiDAR was off, the standard deviations of acceleration on x-axis, y-axis, z-axis were 0.0032 m/s^2, 0.0032 m/s^2, 0.0034 m/s^2, which were on the same level of the standard deviations obtained from AGV platform. When the LiDAR was on, the standard deviations of acceleration on x-axis, y-axis, z-axis were 0.0112 m/s^2, 0.0092 m/s^2, 0.0034 m/s^2, which were much lower than the standard deviations obtained from AGV platform. As shown in Figure 12, the average speed of static drift is 0.0009 m/s on the shelf at point *A*, which was much lower than the average speed of static drift on AGV platform at point *A* in Experiment 1.

The static drift error can be induced by many factors from hardware, such as ranging errors and orientation errors.

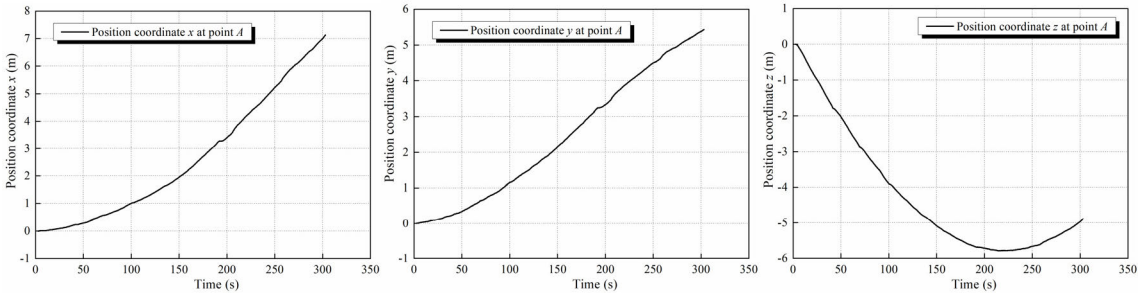

FIGURE 7. Position coordinates at point *A* in Experiment 1.

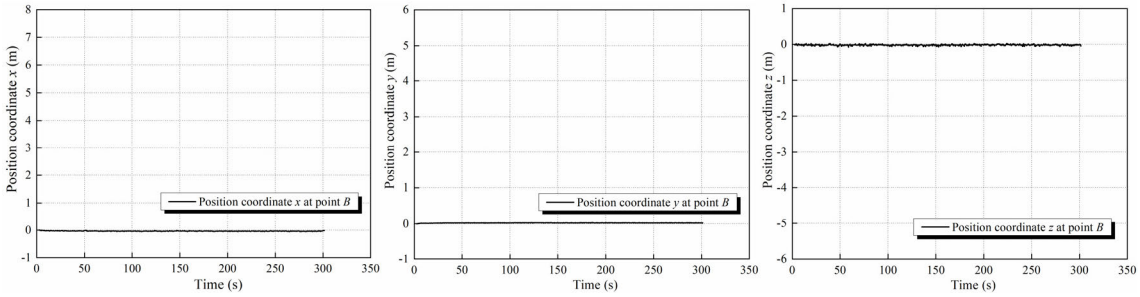

FIGURE 8. Position coordinates at point *B* in Experiment 1.

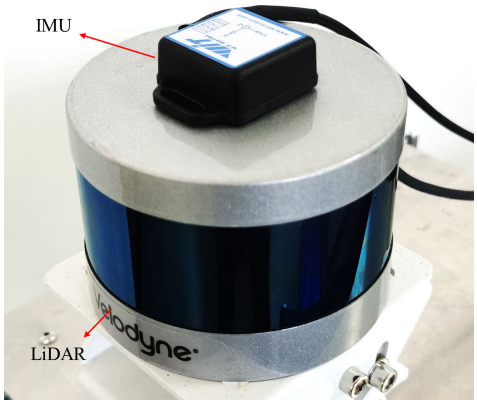

FIGURE 9. Positions of LiDAR and IMU.

According to the results of the contrast experiments, vibration is also a potential inducing factor of static drift. It is necessary to consider the influence of vibration on LiDAR SLAM when the vibration of the platform is evident.

C. CONTRAST EXPERIMENTS ON HARDWARE

The 6-DoF output data of Experiment 2 are shown in Figure 13. The localization output of LOAM is shown as a 3D trajectory in Figure 14. The point cloud map constructed during Experiment 2 is shown in Figure 15.

From Figure 14 and Figure 15, it can be depicted that the localization procedure and mapping procedure of LOAM are both affected by the static drift in the first static phase. The LiDAR can only return to a drifted point A' instead of actual point A at the end of Experiment 2. The final positioning error of the LOAM, i.e., the distance between the initial pose and the final pose, was 3.4154 m.

Both the localization and mapping output of LOAM drifted at point A in the first static phase. The point cloud map of the corridor, which was obtained in the second moving phase, subsequently drifted based on the drifted map of the office. The drift of point cloud map will lead to a serious problem that graph-based optimization methods can only be implemented based on a drifted map. The effect of graph-based optimization methods therefore will be limited.

The static drift can be induced by hardware such as mechanical vibration, ranging measurement errors, and orientation inaccuracy. It would be difficult to perform a contrast experiment with no influence of hardware errors. To overcome the limitation of hardware, the point cloud data can be processed to simulate a LiDAR without hardware errors during static drift in Experiment 2.

The output data of VLP-16 were first identified based on the actual start time and end time of the moving phase in Experiment 2. If the point cloud data are identified as in the state of static drift according to its time stamp, it will be replaced by the point cloud data before the static drift and sent to the SLAM algorithm. If the point cloud data are identified as in the state of normal moving, it will be sent to the SLAM algorithm directly. Therefore, the same point cloud data will be sent to the SLAM algorithm to simulate a LiDAR without any hardware errors during the static drift in the simulated Experiment 2.

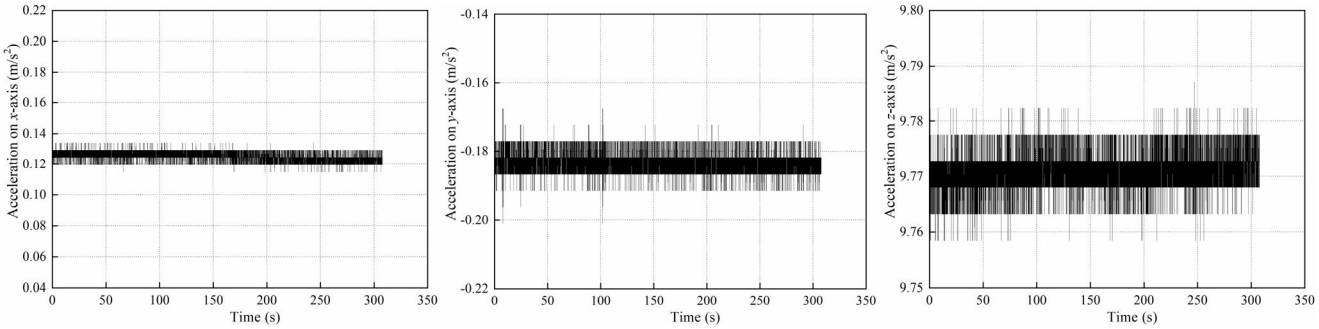

FIGURE 10. Acceleration on *x*-axis, *y*-axis, and *z*-axis when the LiDAR is off.

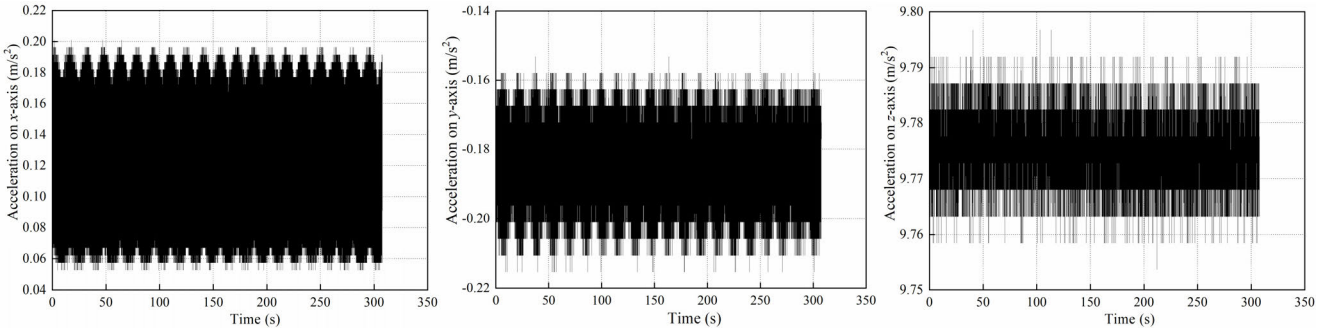

FIGURE 11. Acceleration on *x*-axis, *y*-axis, and *z*-axis when the LiDAR is on.

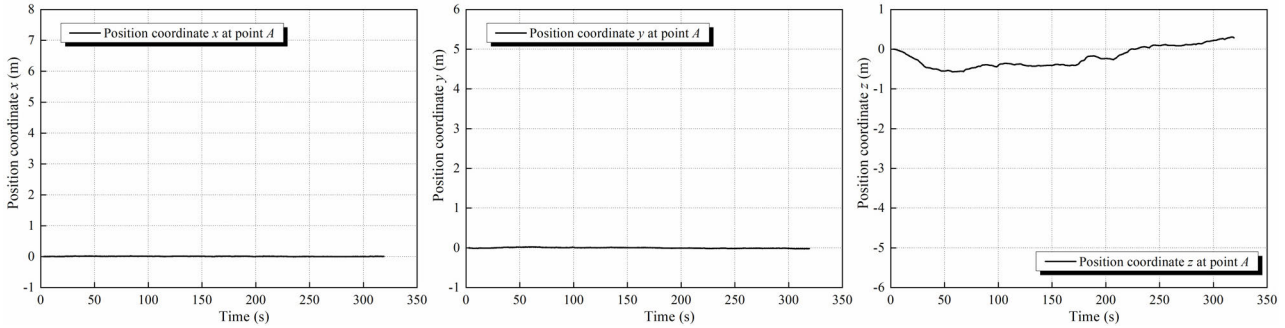

FIGURE 12. Position coordinates at point *A* when the vibration is constrained for contrast.

As shown in Figure 16 and Figure 17, the trajectory and point cloud map of simulated Experiment 2 are all kept on the *x*-*y* plane. The final positioning error of LOAM was reduced from 3.4154 m to 1.1366 m.

From the contrast experiments on hardware, it can be concluded that, though the point cloud was distributed unevenly, a major part of the drift in localization and mapping can be eliminated when the errors from hardware was eliminated. Hence, environment and hardware error are two important inducing factors of static drift. Since both the localization and mapping results of LiDAR SALM can be affected by the static drift and the inducing factors are inevitable during the common use, it is important to identify the existence of static drift and build an algorithm to compensate it.

IV. IDENTIFICATION OF STATIC DRIFT BASED ON KALMAN FILTER

A. KALMAN FILTER DESIGN

Before any compensation measures are implemented, it is essential to identify whether the LiDAR is in the state of static drift. Since the information from odometry and navigation commands are not always available for the identification of static state in all the situations. It is necessary to implement the identification based on the output of LiDAR SLAM. According to Figure 13, parts of the localization output were changing at a relatively steady but low speed during static drift. Therefore, a KF is designed to estimate the speed and acceleration parameters which can be used to identify the existence of static drift. The identification method and pose

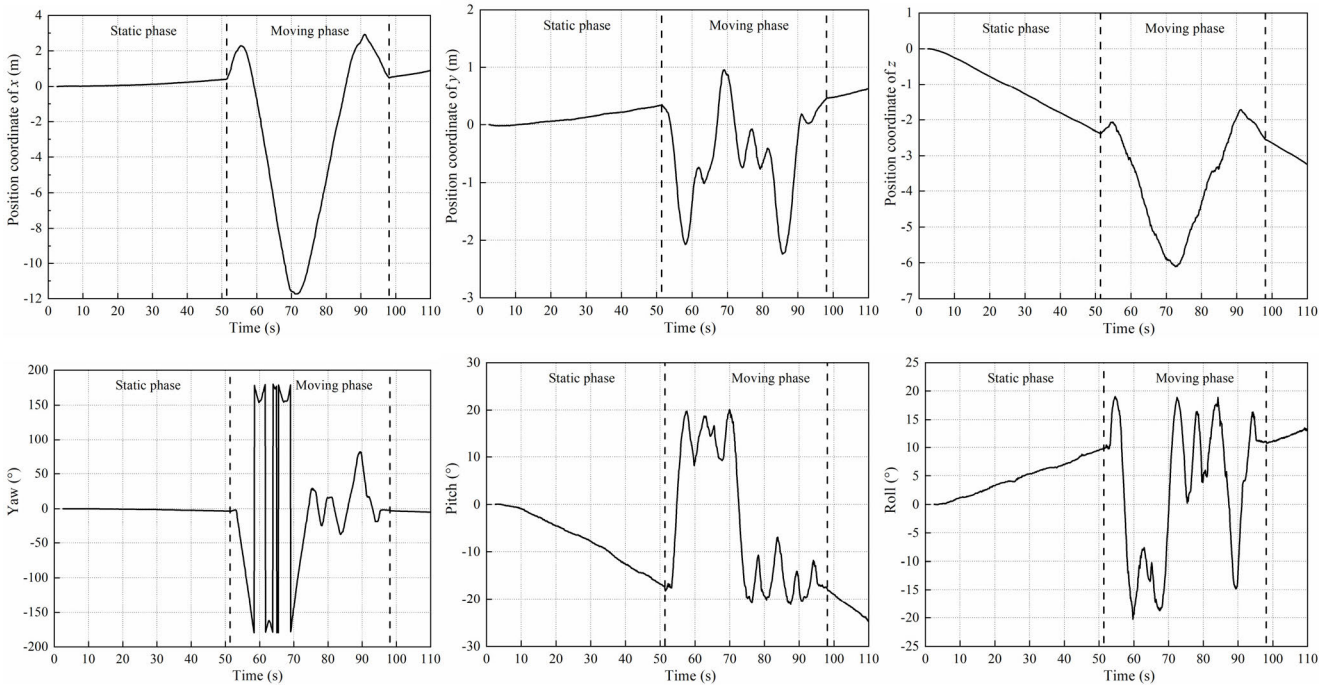

FIGURE 13. 6-DoF output data of LOAM in Experiment 2.

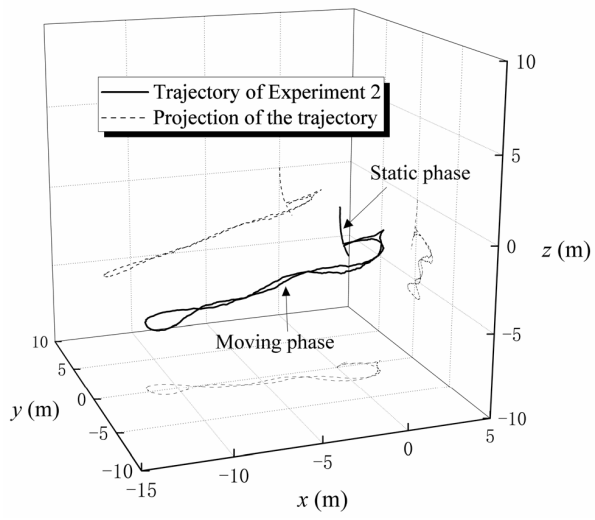

FIGURE 14. 3D trajectory of LOAM in Experiment 2.

compensation method proposed in this paper are aimed to be effective for various platforms in universal scenarios. Hence, all 6-DoF speed and acceleration information are essential to build an estimation criterion of static drift, which can distinguish the static drift from uniform translation along one axis and uniform rotation around one axis.

The state vector in the KF is defined as

$$\begin{aligned}\boldsymbol{x} &= (p, v, a)^{\mathrm{T}} \\ &= (p_x, v_x, a_x, p_y, v_y, a_y, p_z, v_z, a_z, p_{\mathrm{yaw}}, v_{\mathrm{yaw}}, \\ &\quad a_{\mathrm{yaw}}, p_{\mathrm{pitch}}, v_{\mathrm{pitch}}, a_{\mathrm{pitch}}, \mathrm{p}_{\mathrm{roll}}, v_{\mathrm{roll}}, a_{\mathrm{roll}})^{\mathrm{T}} \end{aligned} \quad (1)$$

where p is the position coordinate or rotating angle, v is the velocity and a is the acceleration.

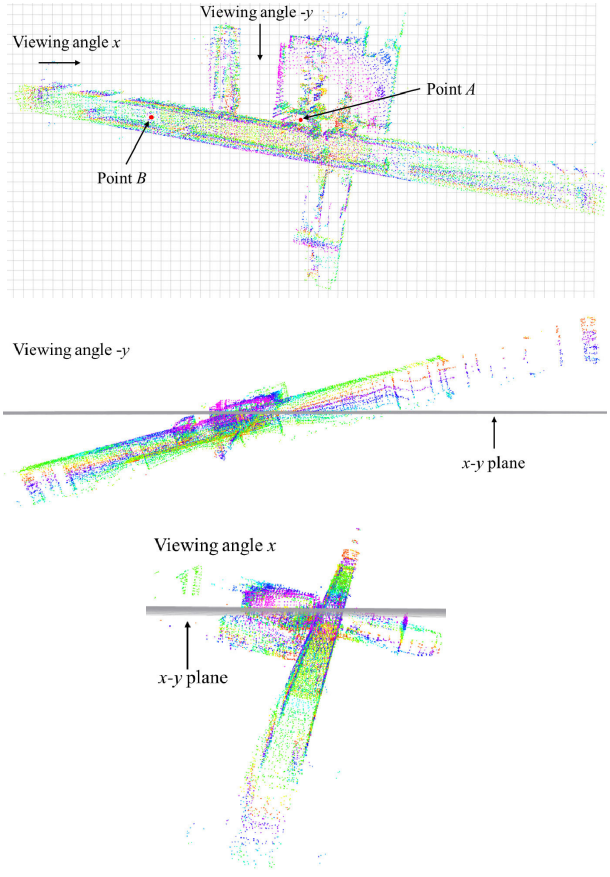

FIGURE 15. Point cloud map constructed in the Experiment 2.

The 18-dimentional state equation can be expressed as

$$\boldsymbol{x}_k = \boldsymbol{F}_k \boldsymbol{x}_{k-1} + \boldsymbol{w} \quad (2)$$

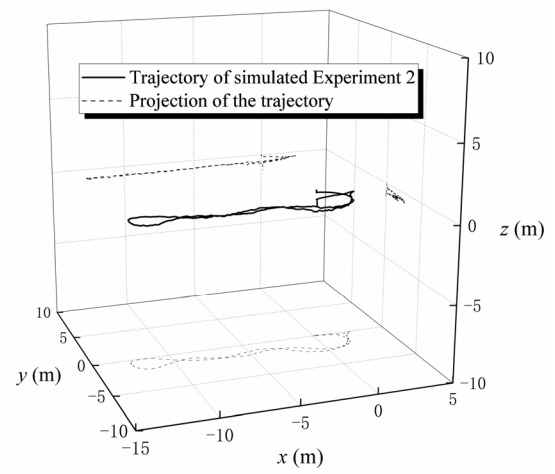

FIGURE 16. 3D trajectory of simulated Experiment 2.

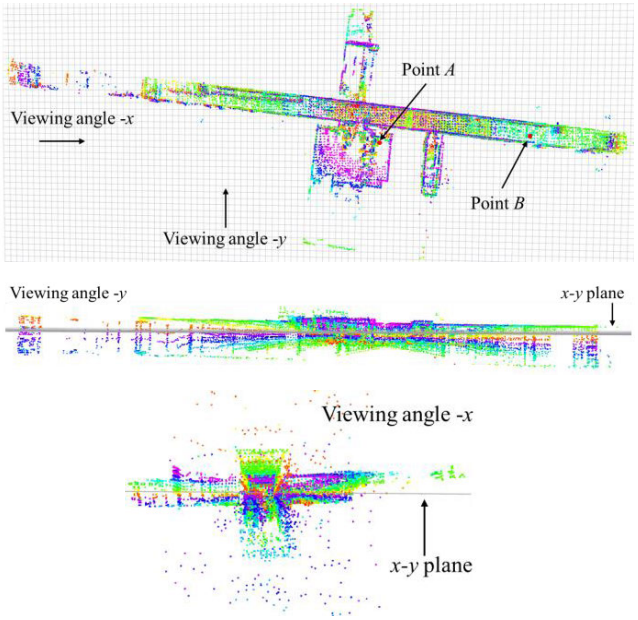

FIGURE 17. Point cloud map constructed in simulated Experiment 2.

where $\boldsymbol{F}_k$ represents the state transition matrix. $\boldsymbol{w}$ represents the system noise which obeys a Gaussian distribution

$$\boldsymbol{w} \sim N(0, \boldsymbol{Q}) \tag{3}$$

where $\boldsymbol{Q}$ represents the processing noise.

The prediction model for one degree of freedom is defined as

$$p_k = p_{k-1} + v_{k-1}\Delta t + \frac{1}{2}a_{k-1}\Delta t^2 \tag{4}$$

where p_k is the position coordinate or rotating angle of current scan, p_{k-1} is the position coordinate or rotating angle of last scan, v_{k-1} is the velocity of last scan, a_{k-1} is the acceleration of last scan, and Δt is the time interval between last scan and current scan.

TABLE 1. The estimation criterion of static drift.

-	x	y	z	yaw	pitch	roll
Maximum absolute value of speed	0.08	0.08	0.136	0.03	0.026	0.04
Maximum absolute value of acceleration	0.1	0.05	0.05	0.02	0.018	0.02

The measurement model for update is expressed as

$$\boldsymbol{z}_k = \boldsymbol{H}_k\boldsymbol{x}_{k-1} + \boldsymbol{y} \tag{5}$$

where $\boldsymbol{z}_k$ represents the observation vector and $\boldsymbol{H}$ represents the measurement function matrix. The $\boldsymbol{y}$ obeys a Gaussian distribution

$$\boldsymbol{y} \sim N(0, \boldsymbol{R}) \tag{6}$$

where $\boldsymbol{R}$ represents the measurement noise.

$\boldsymbol{H}$ is given as

$$H_{i,j} = \begin{cases} 1, & \text{if } i = j = 1, 4, 7, 10, 13, 16 \\ 0, & \text{otherwise} \end{cases} \tag{7}$$

The 6-DoF output data of current scan will be used for update. Therefore, the speed and acceleration parameters of current can be estimated after update.

B. IDENTIFICATION RESULTS

The 6-DoF speed values and the acceleration values in Experiment 2 can be obtained using a KF, as shown in Figure 18 and Figure 19. The estimation criterion should be built according to the characteristics of the external disturbance. The external disturbances, which induced the static drift in our cases, was embodied as a continuous, relatively steady, but slight change in speed and acceleration. Therefore, as listed in Table 1, the estimation criterion of static drift can be established according to the fluctuation range of 6-DoF speed values and acceleration values in Experiment 2.

All 6-DoF data points of Experiment 2 can be identified based on the estimation criterion of static drift. As shown in Figure 20, red dots represent the data points identified as drifting points, and black hollow circles stand for normal data points. The identification accuracy of 1065 points was 99.15% with 9 misidentified points.

V. COMPENSATION ALGORITHM FOR LIDAR SLAM

A. COMPUTATIONAL PROCEDURE

The compensation algorithm's key idea is to identify the start point and end point of each static drift. Then, once the latest drift ends, the compensation matrix will be constantly updated using the pose change from the start point to end point. The pose before the current static drift began will be assigned to the pose of a drifting point. The pose of a normal point, which is not drifting, will be compensated using the compensation matrix to eliminate the pose changes in previous static drifts.

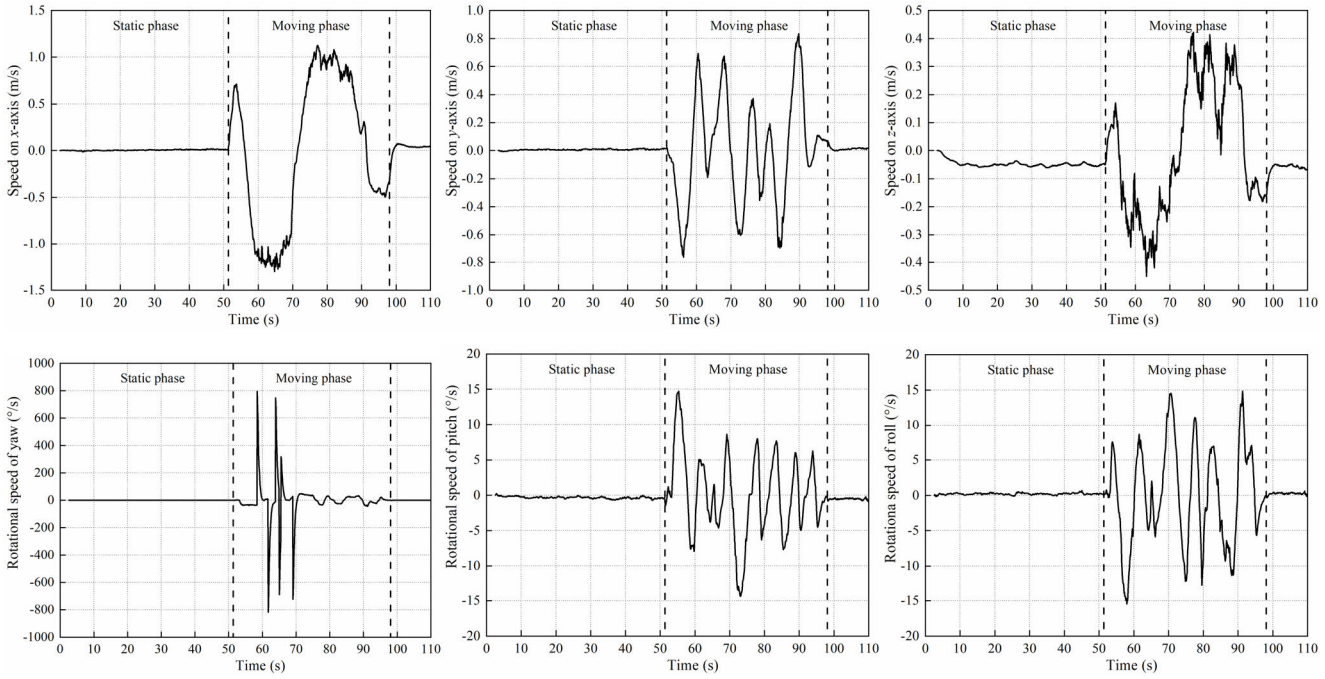

FIGURE 18. 6-DoF speed output of KF for Experiment 2.

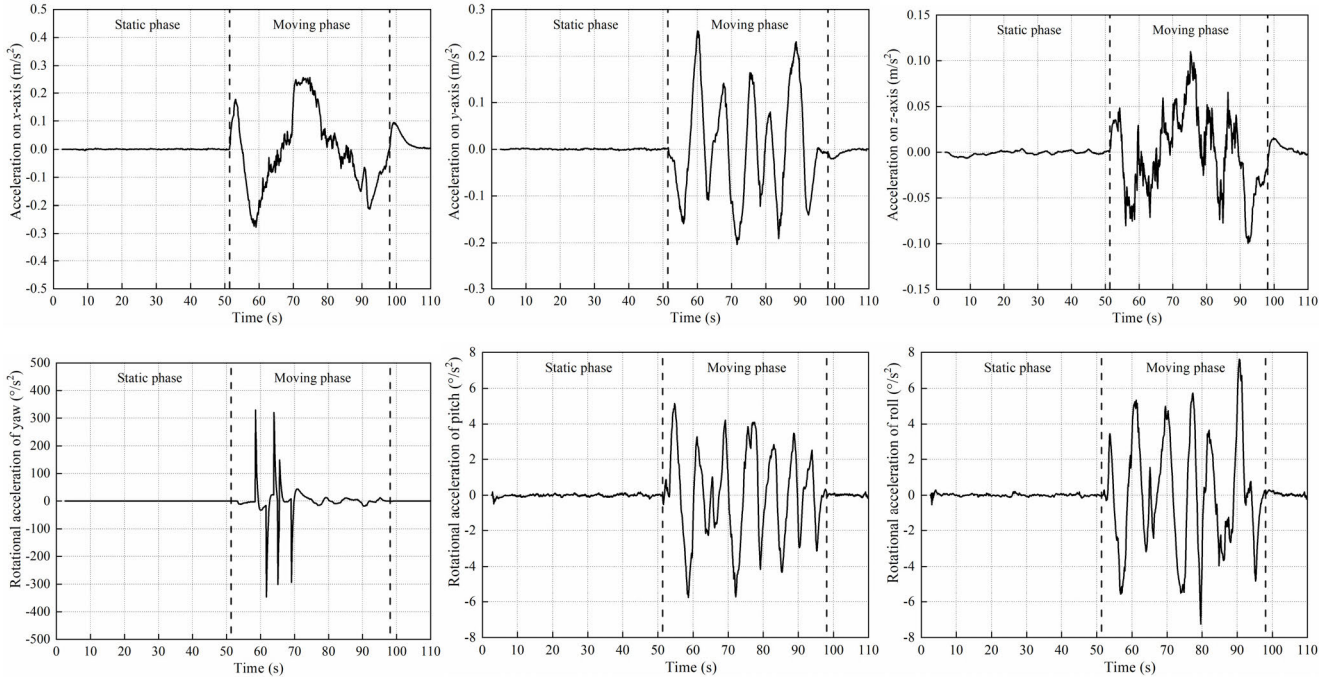

FIGURE 19. 6-DoF acceleration output of KF for Experiment 2.

The computational procedure of the compensation method for static drift is shown in Algorithm 1. The state vector $\boldsymbol{x}_k$ updated by KF was used to estimate whether the current point is a drifting point based on the estimation criterion of static drift.

If the current point is a drifting point, compensated pose of the last point will be assigned to the current point. Furthermore, if the last point is not a drifting point, the current point will be marked as the start point of the current drift.

If the current point is not a drifting point, current point's compensated pose will be calculated using the latest updated compensation matrix. In addition, if the last point is a drifting point, the current point will be marked as the end point of last drift. The compensation matrix will be updated using the pose change from start points to end points in the last drifts.

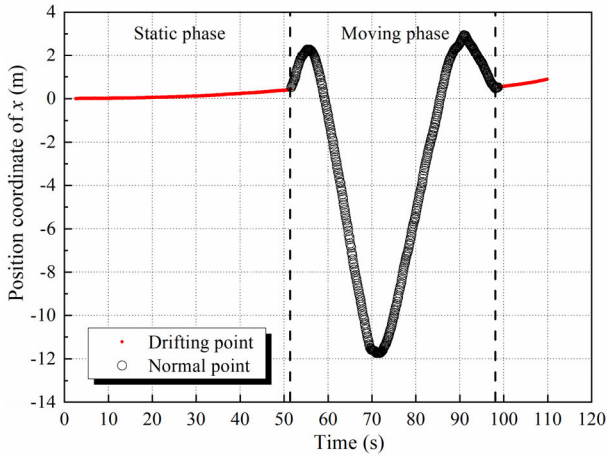

FIGURE 20. Static drift identification of data points (p_x) from the two-phase Experiment 2.

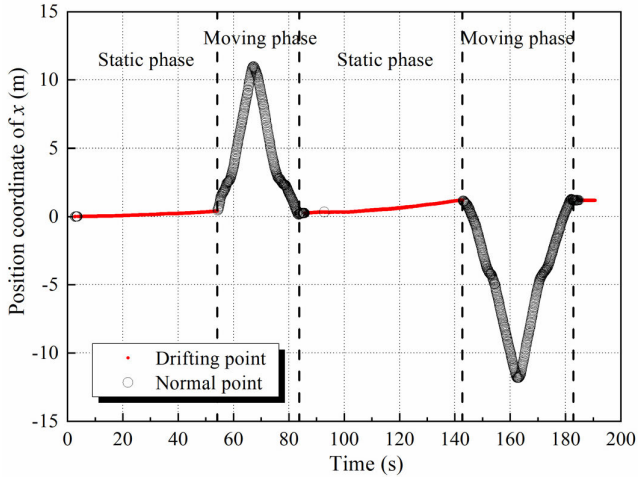

FIGURE 21. Static drift identification of data points (p_x) from Experiment 3.

B. COMPENSATION RESULTS

The identification result of Experiment 3 is shown in Figure 21. The identification accuracy of 1866 points is 97.32% with 50 misidentified points.

Original 6-DoF output data and 6-DoF compensated data of LOAM in Experiment 3 are shown in Figure 22. The consistency of the output data was well preserved after the compensation. Original 3D trajectory and compensated 3D trajectory are shown in Figure 23. In Experiment 3, the final pose of UGV was restored to the initial pose. However, the final position of LOAM was 4.9464 m away from the initial position. After compensation, the distance between final pose and initial pose in Experiment 3 is reduced by 96.48% to 0.1741 m.

VI. DISCUSSION AND FUTURE WORK

A. POTENTIAL INFLUENCE ON LOOP CLOSURE DETECTION

In Experiment 4, the point cloud map of the corridor was constructed twice to investigate the influence of static drift

Algorithm 1 The Computational Procedure of Compensation Method for Static Drift

Input: Observation vector z_k and state vector x_k updated by the KF

Output: Compensated observation vector $z_{k(\text{compensated})}$

if x_k is estimated as a drifting point by the criterion
  Return $z_{k(\text{compensated})} = z_{k-1(\text{compensated})}$
  Mark current data point as a drifting point;
  if the last point is not a drifting point
    Mark current point as a starting point of current drift;
  end if
else
  if the last point is a drifting point
    Mark current point as the end point of last drift;
    Update the compensation matrix using the pose change from the start point to end point for last drift;
  end if
  Calculate the $z_{k(\text{compensated})}$ using z_k and compensation matrix
  Return $z_{k(\text{compensated})}$
end if

on the mapping process. When the LiDAR enters a visited environment after a period of static drift, the interference in mapping procedure can lead to various consequences. If the LiDAR has not drifted far away from the previous map, it may be possible for the LiDAR to find its location back in the previous map. If the LiDAR has drifted far enough from the previous map, such as in the case of Experiment 4 (Figure 24), a new map of the visited environment will be constructed at a drifted position (Figure 25).

According to the results of Experiment 4, the static drift can severely affect the mapping process of the SLAM algorithm, which would further obstruct the subsequent graph-based optimization algorithms, such as loop closure detection.

Since the identification of static drift can be performed using only the localization results of last scan and current scan, the identification and compensation algorithms can be implemented into the SLAM algorithm in the future work. Then, the point cloud affected by static drift can be prevented from being updated into the global map.

B. STATIC DRIFT AFTER GROUND DETECTION BEING IMPLEMENTED

LeGO-LOAM was proposed by Shan and Englot [16], which leverages ground separation, point cloud segmentation, and improved Levenberg-Marquardt optimization. To investigated its performance under the influence of static drift, LeGO-LOAM was tested with the same input data from conducted experiments.

The output data of p_z in Experiment 1 using LeGO-LOAM are shown in Figure 26 and Figure 27, which indicates the existence of static drift at point A. But the speed of static

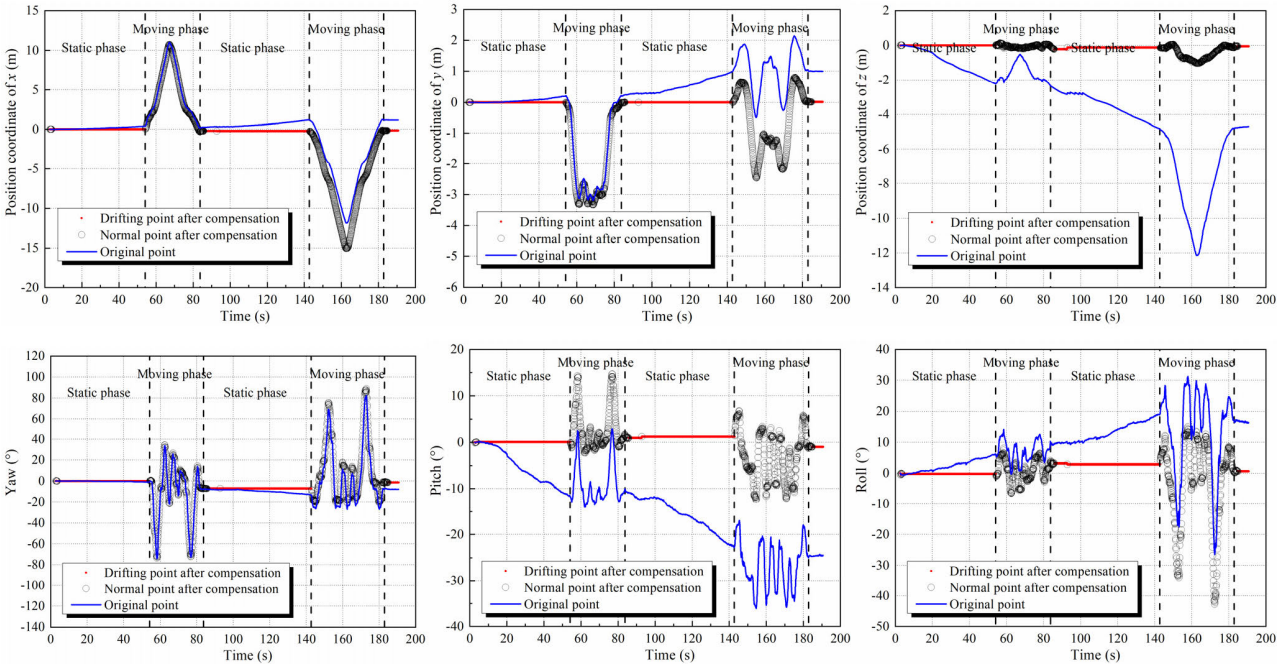

FIGURE 22. Original 6-DoF output data and compensated 6-DoF data of Experiment 3.

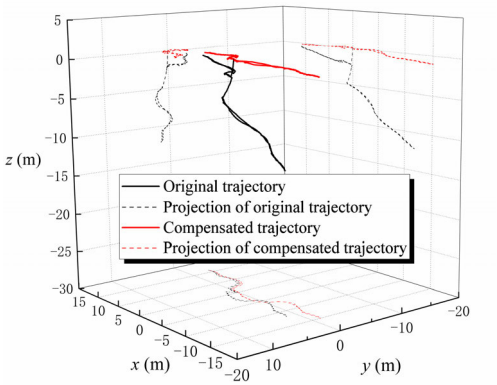

FIGURE 23. Original 3D trajectory and compensated 3D trajectory of Experiment 3.

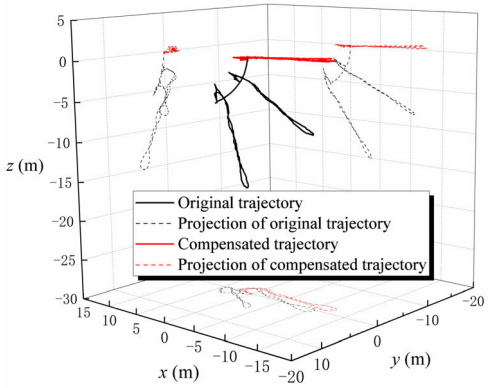

FIGURE 24. 3D trajectory of Experiment 4.

drift for LeGO-LOAM was much lower than the speed of static drift for LOAM according to the comparison between Figure 7 and Figure 27. The average speed of static drift for LeGO-LOAM at point *A* was 0.0032 m/s.

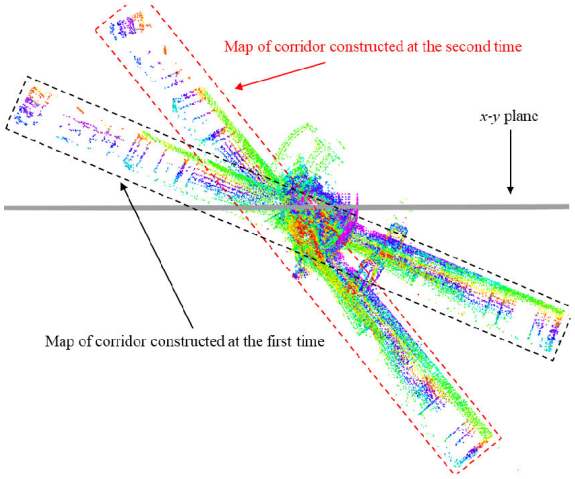

FIGURE 25. Point cloud map constructed in Experiment 4.

The 6-DoF output data of Experiment 3 using LeGO-LOAM are shown in Figure 28. The point cloud map constructed in Experiment 3 using LeGO-LOAM is shown in Figure 29. The final positioning error of the LeGO-LOAM was found to be 0.8341 m, which was lower than LOAM.

Due to the optimization based on ground detection, the performance of LeGO-LOAM was more stable than LOAM under the influence of static drift. However, according to Figure 28 and Figure 29, the influence of static drift on the output of localization and mapping still existed after the graph-based optimization being implemented in LeGO-LOAM. When the external disturbances become severer and

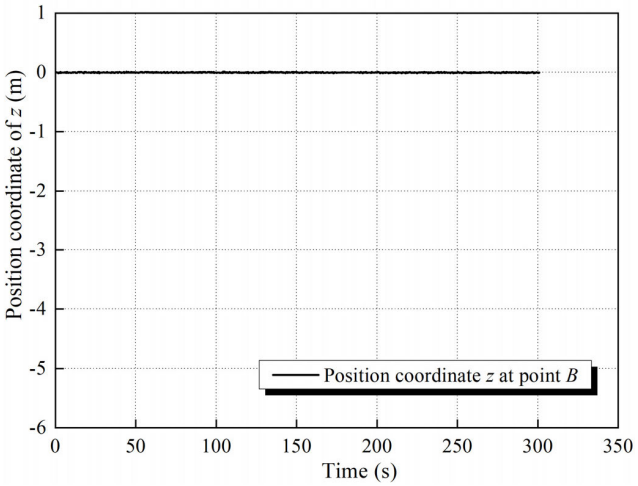

FIGURE 26. Position coordinate of z at point B in Experiment 1 using LeGO-LOAM.

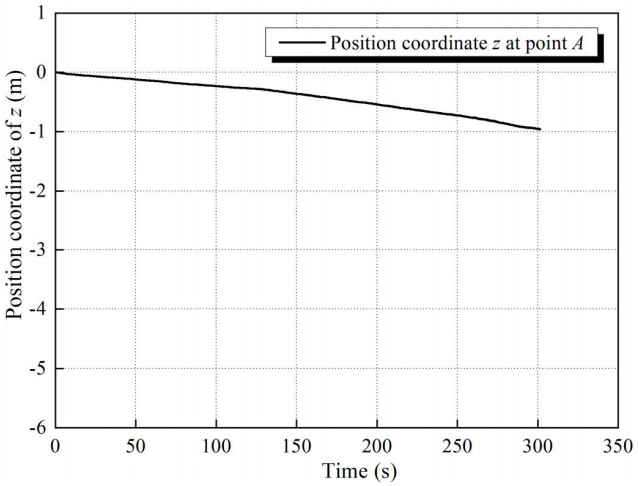

FIGURE 27. Position coordinate of z at point A in Experiment 1 using LeGO-LOAM.

the error sources become more complicate, the influence on the output of LeGO-LOAM can be more significant.

Furthermore, ground detection may not be available under extreme conditions. It can be difficult to extract ground, when a LiDAR mounted on a tractor operates over rough terrains and on off-road surfaces, or when a LiDAR mounted on a plane conducts aerial survey in mountain areas. It is necessary to adopt methods against certain dominant disturbances under certain conditions, which could be an important supplement to extending the use of LiDAR SLAM in various areas.

The point cloud distribution in the environment can provide constrains for the static drift and the dynamic drift. Unevenly distributed point cloud in a certain environment should be given more attention in the use of LiDAR SLAM.

For other platforms, such as cars and UAVs, the static drift can be affected by various kinds of external disturbances. The feature of static drift can also be different accordingly. In order to achieve an adequate accuracy, the estimation criterion of static drift should be adjusted according to different SLAM algorithms, different environments, and different hardware conditions.

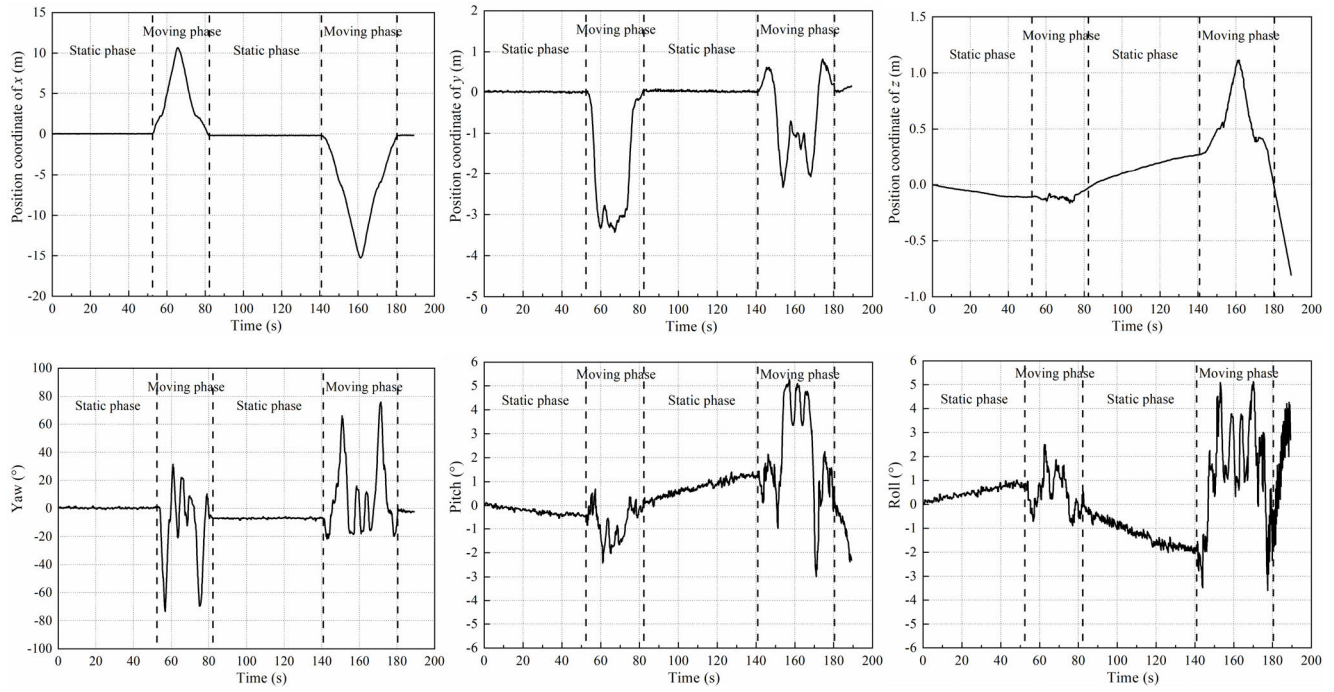

FIGURE 28. 6-DoF output data of LeGO-LOAM in Experiment 3.

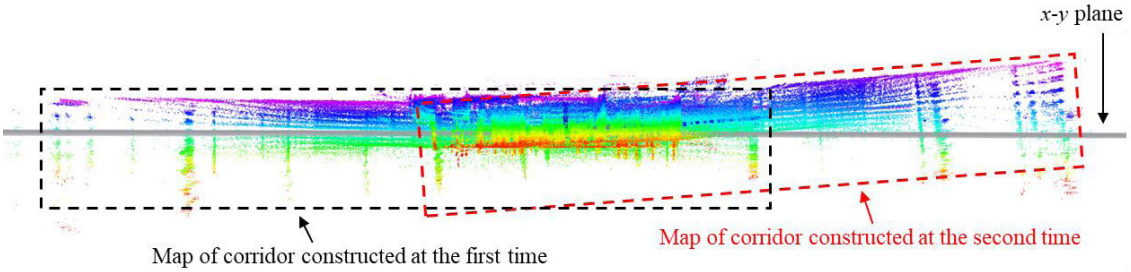

FIGURE 29. Point cloud map constructed in Experiment 3 using LeGO-LOAM.

VII. CONCLUSION

In this study, the inducing factors of static drift were evaluated by experiments. An identification method based on parameter estimation and a compensation algorithm were proposed to eliminate the static drift influence on LiDAR SLAM. The main results are summarized as follows:

(1) Environment is an inducing factor of static drift based on the results of experiments at different locations. Static drift of LOAM can be observed with the average drift speed of 0.0333 m/s when the point cloud was not distributed uniformly in the environment.

(2) Besides the ranging measurement error and the orientation error, vibration is also a potential inducing factor of static drift according to the results of contrast experiments. The localization and mapping results of LiDAR SALM in Experiment 2 was affected by the static drift. In the simulated Experiment 2, when the influence of hardware errors during the static drift was entirely filtered, the final positioning error was reduced from 3.4154 m to 1.1366 m.

(3) A KF was built to estimate the speed and acceleration parameters of LiDAR SLAM based on the localization results of SLAM. An estimation criterion for the identification of static drift can be established based on the value ranges of speed and acceleration during a static drift. For 1065 points in Experiment 2, the identification accuracy was 99.15%.

(4) A compensation algorithm for static drift was proposed. Based on the estimation criterion, static drifts in Experiment 3 were identified and compensated. For 1866 points, the identification accuracy was 97.32%, and the final positioning error was reduced from 4.9464 m to 0.1741 m.

REFERENCES

[1] Z. Hui, S. Jin, P. Cheng, Y. Y. Ziggah, L. Wang, Y. Wang, H. Hu, and Y. Hu, "An active learning method for DEM extraction from airborne LiDAR point clouds," *IEEE Access*, vol. 7, pp. 89366–89378, 2019, doi: 10.1109/ACCESS.2019.2926497.

[2] T. F. Canata, J. P. Molin, and R. V. D. Sousa, "A measurement system based on LiDAR technology to characterize the canopy of sugarcane plants," *Engenharia Agrícola*, vol. 39, no. 2, pp. 240–247, Apr. 2019, doi: 10.1590/1809-4430-eng.agric.v39n2p240-247/2019.

[3] F. Taubert, R. Fischer, N. Knapp, and A. Huth, "Deriving tree size distributions of tropical forests from LiDAR," *Remote Sens.*, vol. 13, no. 1, p. 131, Jan. 2021, doi: 10.3390/rs13010131.

[4] Z. Li, Y. Yan, Y. Jing, and S. G. Zhao, "The design and testing of a LiDAR Platform for a UAV for heritage mapping," *ISPRS Int. Arch. Photogramm., Remote Sens. Spatial Inf. Sci.*, vols. XL-1–W4, no. 4, pp. 17–24, Aug. 2015, doi: 10.5194/isprsarchives-XL-1-W4-17-2015.

[5] P. J. Besl and N. D. McKay, "A method for registration of 3-D shapes," *IEEE Trans. Pattern Anal. Mach. Intell.*, vol. 14, no. 2, pp. 239–256, Feb. 1992, doi: 10.1109/34.121791.

[6] J. Zhang and S. Singh, "LOAM: Lidar odometry and mapping in real-time," *Robot., Sci. Syst.*, vol. 2, no. 9, pp. 1–9, Jul. 2014, doi: 10.15607/RSS.2014.X.007.

[7] J. Zhang and S. Singh, "Low-drift and real-time Lidar odometry and mapping," *Auton. Robots*, vol. 41, no. 2, pp. 401–416, Feb. 2017, doi: 10.1007/s10514-016-9548-2.

[8] M.-L. Li, Y.-H. Hu, N.-X. Zhao, and Q.-S. Qian, "Modeling and analyzing point cloud generation in missile-borne LiDAR," *Defence Technol.*, vol. 16, no. 1, pp. 69–76, Feb. 2020, doi: 10.1016/j.dt.2019.10.003.

[9] J. Kolecki, M. Prochaska, Z. Kurczyński, P. Piątek, and J. Baranowski, "Developing the stabilized mapping system for the gyrocopter-report from the first tests," *ISPRS Int. Arch. Photogramm. Remote Sens. Spat. Inf. Sci.*, vols. XLI–B1, pp. 31–36, Jun. 2016, doi: 10.5194/isprsarchives-XLI-B1-31-2016.

[10] W. Luo and L. Li, "Automatic geometry measurement for curved ramps using inertial measurement unit and 3D LiDAR system," *Autom. Construct.*, vol. 94, pp. 214–232, Oct. 2018, doi: 10.1016/j.autcon.2018.07.004.

[11] C. F. Periu, A. Mohsenimanesh, C. Laguë, and N. B. McLaughlin, "Isolation of vibrations transmitted to a LiDAR sensor mounted on an agricultural vehicle to improve obstacle detection.," *Can. Biosyst. Eng.*, vol. 55, no. 1, pp. 2.33–2.42, Dec. 2013, doi: 10.7451/CBE.2013.55.2.33.

[12] S. Thrun and M. Montemerlo, "The graph SLAM algorithm with applications to large-scale mapping of urban structures," *Int. J. Robot. Res.*, vol. 25, nos. 5–6, pp. 403–429, May 2006, doi: 10.1177/0278364906065387.

[13] R. Dong, Z.-G. Wei, C. Liu, and J. Kan, "A novel loop closure detection method using line features," *IEEE Access*, vol. 7, pp. 111245–111256, 2019, doi: 10.1109/ACCESS.2019.2934521.

[14] G. Zhang, X. Yan, and Y. Ye, "Loop closure detection via maximization of mutual information," *IEEE Access*, vol. 7, pp. 124217–124232, 2019, doi: 10.1109/ACCESS.2019.2937967.

[15] Y. Li, Z. Hu, G. Huang, Z. Li, and M. A. Sotelo, "Image sequence matching using both holistic and local features for loop closure detection," *IEEE Access*, vol. 5, pp. 13835–13846, 2017, doi: 10.1109/ACCESS.2017.2725387.

[16] T. Shan and B. Englot, "LeGO-LOAM: Lightweight and ground-optimized LiDAR odometry and mapping on variable terrain," in *Proc. IEEE/RSJ Int. Conf. Intell. Robots Syst. (IROS)*, Oct. 2018, pp. 4758–4765, doi: 10.1109/IROS.2018.8594299.

[17] H. Pu, S. Yuan, Y. Peng, K. Meng, J. Zhao, R. Xie, Y. Huang, Y. Sun, Y. Yang, S. Xie, J. Luo, and X. Chen, "Multi-layer electromagnetic spring with tunable negative stiffness for semi-active vibration isolation," *Mech. Syst. Signal Process.*, vol. 121, pp. 942–960, Apr. 2019, doi: 10.1016/j.ymssp.2018.12.028.

[18] Y. Liu, N. Nogichi, and K. Ishii, "Development of a small-sized and low-cost attitude measurement unit for agricultural robot application," *Tarim Bilimleri Dergisi*, vol. 24, no. 1, pp. 33–41, Apr. 2018, doi: 10.15832/ankutbd.446369.

[19] H. Peng, X. Zhi, R. Wang, J.-Y. Liu, and C. Zhang, "A new dynamic calibration method for IMU deterministic errors of the INS on the hypersonic cruise vehicles," *Aerosp. Sci. Technol.*, vol. 32, no. 1, pp. 121–130, Jan. 2014, doi: 10.1016/j.ast.2013.11.005.

[20] A. R. Jiménez, F. Seco, F. Zampella, J. C. Prieto, and J. Guevara, "PDR with a foot-mounted IMU and ramp detection," *Sensors*, vol. 11, no. 10, pp. 9393–9410, Sep. 2011, doi: 10.3390/s111009393.
[21] Z. Tao, W. Chengcheng, and Y. Jie, "Research on indoor positioning technology based on MEMS IMU," in *Artificial Intelligence and Robotics*, vol. 752. Cham, Switzerland: Springer, 2018, pp. 143–156, doi: 10.1007/978-3-319-69877-9_16.
[22] M. Narasimhappa, A. D. Mahindrakar, V. C. Guizilini, M. H. Terra, and S. L. Sabat, "MEMS-based IMU drift minimization: Sage Husa adaptive robust Kalman filtering," *IEEE Sensors J.*, vol. 20, no. 1, pp. 250–260, Jan. 2020, doi: 10.1109/JSEN.2019.2941273.
[23] N. Song, Z. Yuan, and X. Pan, "Adaptive Kalman filter based on random-weighting estimation for denoising the fiber-optic gyroscope drift signal," *Appl. Opt.*, vol. 58, no. 35, pp. 9505–9513, Dec. 2019, doi: 10.1364/AO.58.009505.
[24] G. Yang, Y. Liu, M. Li, and S. Song, "AMA-and RWE-based adaptive Kalman filter for denoising fiber optic gyroscope drift signal," *Sensors*, vol. 15, no. 10, pp. 26940–26960, Oct. 2015, doi: 10.3390/s151026940.
[25] R. Peesapati, S. L. Sabat, K. P. Karthik, J. Nayak, and N. Giribabu, "Efficient hybrid Kalman filter for denoising fiber optic gyroscope signal," *Optik*, vol. 124, no. 20, pp. 4549–4556, Oct. 2013, doi: 10.1016/j.ijleo.2013.02.013.

DA LI received the bachelor's and Ph.D. degrees in aerospace propulsion theory and engineering from Beihang University, China, in 2012 and 2017, respectively. He is currently a Postdoctoral Research Associate in traffic and transportation engineering with the School of Transportation Science and Engineering, Beihang University. His research interests include LiDAR SLAM and localization based on multi-sensor fusion.

BIN ZHOU received the Ph.D. degree from the School of Transportation Science and Engineering, Beihang University, Beijing, China, in 2018. He is currently a Postdoctoral Scholar with the School of Electronic and Information Engineering, Beihang University. His research interests include deep-learning algorithms, intelligent connected vehicle, big data analysis, and traffic network modeling.

ZHANGYU WANG received the M.S. degree in transportation information engineering and control from Beihang University, Beijing, China, in 2018, where he is currently pursuing the Ph.D. degree with the School of Transportation Science and Engineering. His research interests include intelligent vehicle and computer vision.

SONGYUE YANG received the M.S. degree in flight vehicle design from Beihang University, Beijing, China, in 2020, where he is currently pursuing the Ph.D. degree with the School of Transportation Science and Engineering. His research interests include deep reinforcement learning and computer vision.

PENGFEI LIU received the B.E. degree in transportation engineering from Beihang University, Beijing, China, in 2018, where she is currently pursuing the Ph.D. degree with the School of Transportation Science and Engineering. Her research interests include computer vision and data fusion.